CR-114968

spectrolab

A Division of textron Inc.

Report No.	Project No.	Date
3718- Engr. Study	NA59-11114	22 January, 1971

Title: ENGINEERING STUDY
Chamber "D" Solar Simulator

Written By: R.W. Basil, Project Manager — A.C. Brown, Optical Engineer

Approved By: T.J. Shohfi - Program Management Department Manager — M.D. Hoffman for T.J. Shohfi

Approved By: J.D. Gum, Engineering Manager

Status: Preliminary _____ Planning _____

Pretest _____ Progress X Final _____ Revision _____

Summary: This report provides the Engineering study to predict the system performance of the "D" chamber solar simulator system using the "B" chamber source module.

Circulation: NASA/MSC - 9 copies

SPECTROLAB - 6 copies

12484 GLADSTONE AVENUE / SYLMAR, CALIFORNIA 91342 / PHONE (213) 365-4611

CR-114968

Spectrolab

A Division of Textron Inc.

Report No.	Project No.	Date
3718- Engr. Study	NA59-11114	22 January, 1971

Title: ENGINEERING STUDY
Chamber "D" Solar Simulator

Written By: R.W. Basil, Project Manager; A.C. Brown, Optical Engineer

Approved By: T.J. Shohfi - Program Management, Department Manager

Approved By: J.D. Gum, Engineering Manager

Status: Preliminary ____ Planning ____

Pretest ____ Progress X Final ____ Revision ____

Summary: This report provides the Engineering study to predict the system performance of the "D" chamber solar simulator system using the "B" chamber source module.

Circulation: NASA/MSC - 9 copies

SPECTROLAB - 6 copies

Details of illustrations in this document may be better studied on microfiche

PREFACE

OBJECTIVE

The objective of this engineering study was to determine the practicability of utilizing a Chamber "B" xenon source module for the radiation source assembly on the Chamber "D" solar simulator system.

SCOPE OF WORK

This effort was divided into three phases.

In Phase I, the geometric considerations required for successful interchange of optical components were explored. This is covered by Section 1 of this report.

Phase II evaluated the anticipated test volume performance of the Chamber "D" solar simulator system utilizing the Chamber "B" xenon source module.

Phase III, covered in Section 3, investigated the requirements for mechanical interchange of the two source units and the changes necessary for utilities interfacing with the "B" chamber source module.

CONCLUSIONS

The interchange of source modules presents no optical problems. A system efficiency analysis indicates that the Chamber "B" xenon solar module can be utilized to provide a one solar constant irradiance within the Chamber "D" test volume.

Comparison of the outline drawings of the source enclosure for "D" chamber and the source module for "B" chamber suggests that modifications of the enclosure might be relatively uncomplicated. More detailed information about the enclosure, and more specific information concerning the "D" chamber power supply, control console and utilities would be a prerequisite to finalizing specifications.

FIGURES

APPENDIX

DRAWINGS

1.0 OPTICAL COMPATIBILITY

1.1 To determine the feasibility of fitting the B chamber source module into the D chamber solar simulator, it was prerequisite to examine any change of optical geometry which might occur. To assist in the examination the simplified schematic of Figure 1 was constructed. On this figure is shown the ellipsoid "E" and a pair of lenses "L-1" and "L-2". Rays from points on the ellipsoid which penetrate the first lens will penetrate the second lens and form thereon an image of the ellipsoid. This image is the limiting aperture of the system; rays which might penetrate the second lens outside this aperture would become stray light inside the vacuum vessel.

1.2 The solid angle A'OB' formed by the ellipsoid image is equal to the solid angle A OB formed by the ellipsoid; thus, in order to eliminate the possiblity of stray light a replacement collector must fit inside, or match angle A OB . The large aperture of the 24-inch ellipsoid is 23.16 inches diameter; the corresponding dimension of the 22-inch aconic is 22.16 inches. To match the angle of the ellipsoid, which has been assumed to be mounted 50.0 inches from the mosaic lens assembly, the aconic would be installed: $\frac{22.16}{23.16} \times 50.0 = 47.84$ inches from the mosaic lenses.

1.3 Figure 3 illustrates how the B chamber source module might be fitted to the existing enclosure at the solar port of D chamber. By removing the "conical" end of the structure, the new source module could be installed with the aconic collector in the same location as the ellipsoid. This location would obviate geometric problems and would afford better arc utilization than would the 47.84 inch dimension calculated above.

PREPARED BY: A C Brown	spectrolab A Division of [redacted] Inc.	PAGE NO. 2 OF Job No. 3718
CHECKED BY:		REPORT NO.
DATE:	TITLE SIMPLIFIED OPTICAL SCHEMATIC	MODEL NO:

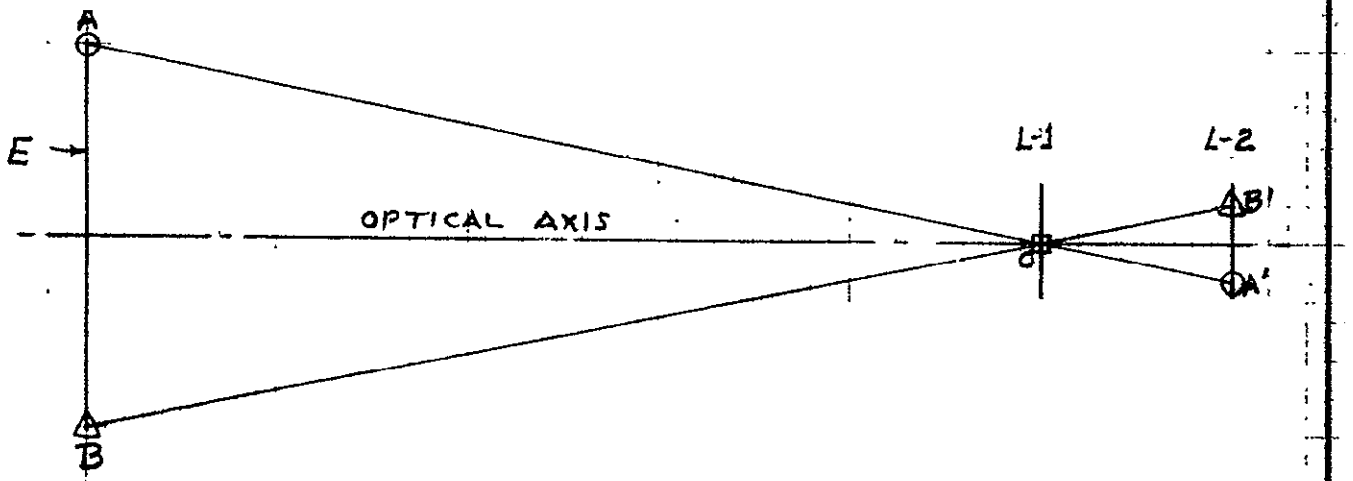

FIG. 1

2.0 PERFORMANCE CONSIDERATIONS

2.1 The probable power input required for the B chamber source module to meet the operating specifications of D chamber was determined by estimating the system efficiency. The method used is the one described in Section 5, pages 5-22 through 5-24, of the "Handbook of Solar Simulation for Thermal Vacuum Testing", published by the Institute of Environmental Sciences; these efficiency factors are also listed and defined in Appendix A.

Results of this determination, listed in Table I, show that required input power to the B chamber source module to be 15.46KW as contrasted to the D chamber source assembly requirement of 12.09KW for one solar constant intensity in the test volume.

2.2 Note that in Table I the two factors which differ are those associated with the only optical element which was changed: the collector. The collection angle of the aconic, 79.8°, is less than the 90.4° angle of the ellipsoid. The aconic surface starts at 52.1° and ends at 131.9°; the ellipsoid surface begins at 45.6° and terminates at 136.0°. The 6.5° starting difference and the 4.1° end difference lie in low energy level regions of the lamp output; thus flux collection of the aconic collector was conservatively estimated to be 94% of that afforded by the ellipsoid.

2.3 The second differing factor is arc image utilization. In the D chamber application the aconic collector is to be used at 50 inches from the mosaic lenses instead of the design distance of 72 inches. As a result the arc utilization factor is considerably degraded. That this loss may be appreciably reduced is shown in Appendix B. In this study, the location of the lamp relative to the collector focus was varied in order to obtain an optimum distribution of lamp energy at the mosaic lenses. Results suggested that the arc utilization factor of the aconic might equal 83% of that of the ellipsoid.

TABLE I

SYSTEM EFFICIENCY COMPARISON

FACTOR *	VALUE	
	ELLIPSOID	ACONIC
Power Conversion	.52	.52
Flux Collection	.80	.75
Collector Reflectance	.86	.86
Obstructions	.98	.98
Arc Utilization	.84	.70
Packing Factor	.84	.84
Lens Transmission	.85	.85
Window Transmission	.92	.92
Spectral Filter	.70	.70
Vignetting and Spillover	.98	.98
Collimating Mirror	.86	.86
System Efficiency	.1141	.0892

Power on target = target area (ft^2) X solar constant/ft^2

Target area = hexagonal - 3.5 ft. across flats

Area = $(3.5 \text{ ft.})^2$ (.8660254) = 10.609 ft^2

Power on target = 10.609 ft^2 X $\frac{.130 \text{ KW}}{Ft^2}$ = 1.3792 KW

Input power = (power on target) $\div$ (system efficiency)

Input power (KW)	ELLIPSOID	ACONIC
	12.0	15.5

* Efficiency factor as listed and explained in section 5 of the "Handbook of Solar Simulation for Thermal Vacuum Testing" and Appendix A.

2.4 Uniformity in the test volume is entirely the result of the integrating action of the mosaic lens assembly. Each individual successive lens pair completely illuminates the test volume, thus the intensities of all lenses are summed in the vacuum vessel. For this reason, the interchange of source modules will not affect test volume uniformity.

3.0 "B" CHAMBER XMH-300 SOURCE MODULE SPECIFICATION FOR "D" CHAMBER UTILIZATION

3.1 Introduction

This specification describes the "B" chamber XMH-300 self-contained Xenon source module (Spectrolab Drawing 019131 and Fig. 2) for illuminating the "D" chamber mosaic lens assembly in the "D" chamber solar simulator. The module is designed around a Xenon short arc lamp source and contains various required components, including the lamp starter, lamp adjusting mechanism, a metal aconic source collector, and all thermal, electrical and environmental control systems necessary to permit long-term safe operation of the lamp. (See Spectrolab Drawing No. 018669).

The XMH-300 is designed to work in conjunction with a power supply capable of meeting the Xenon short arc lamp operating requirements (reference Spectrolab's LC-52).

3.2 Subsystem Description

The XMH-300 is composed of six major subsystems as detailed in the following paragraphs.

3.2.1 Light Source

A high performance 25 KW xenon short arc lamp is used in the XMH-300 source module. The lamp utilizes tungsten anodes with high speed cooling passages and an aerodynamic cathode to minimize arc/boundary layer interactions.

3.2.2 Starter

The XMH-300 is provided with a 70 KV starter to ignite the lamp. Lamp starting is provided by a 115V AC signal to the

PREPARED BY: R.V. Basil	**spectrolab** A Division of EXTRON Inc.	PAGE NO. 7 OF
CHECKED BY:		Job No. 3718 REPORT NO.
DATE: 15 JAN., 71	TITLE MSC "B" CHAMBER XMH-300-INVERTED	MODEL NO. XMH-300

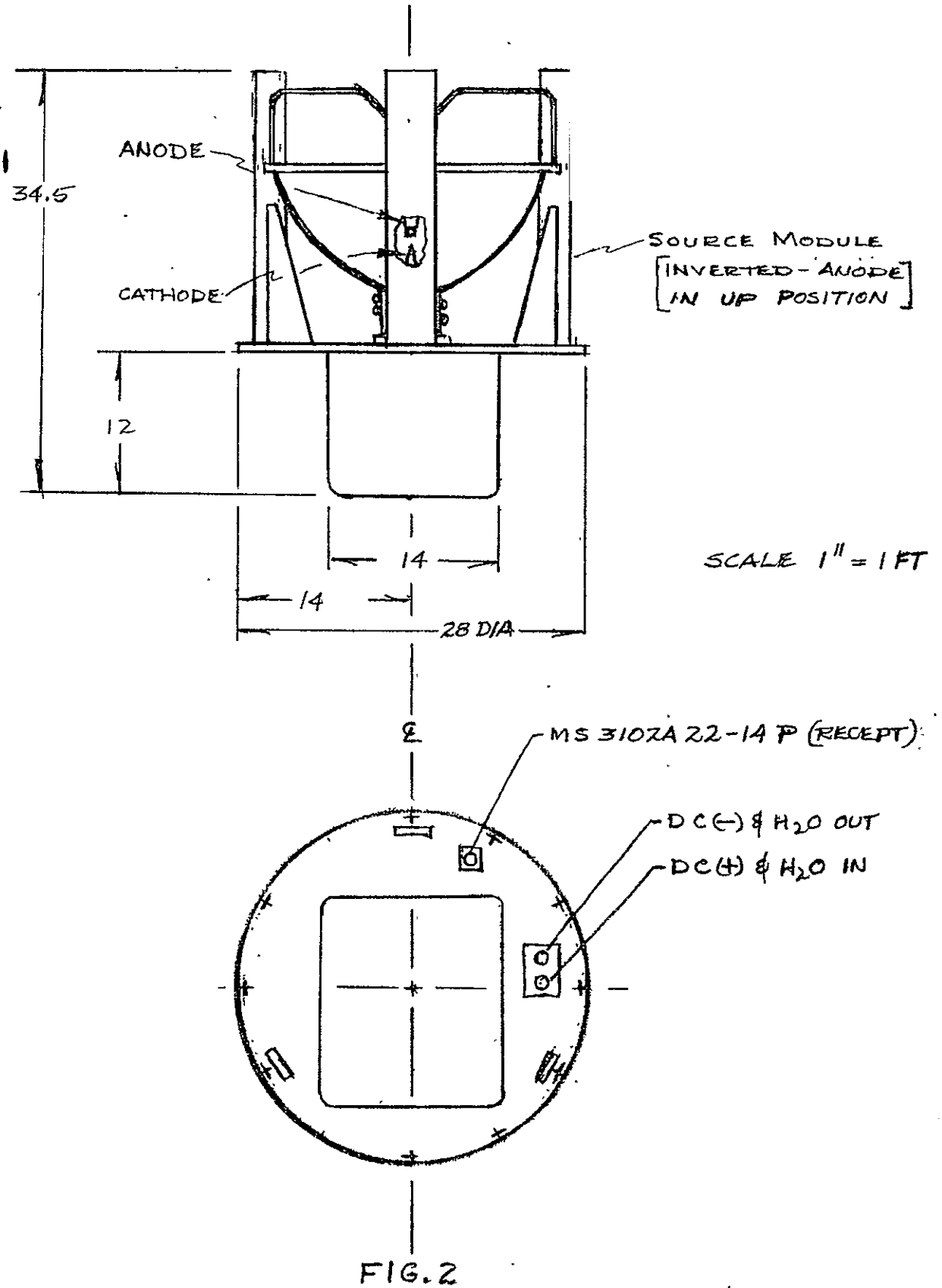

FIG. 2

NOTE SEE S/L DWG 019131

starter circuit. Upon starting of the lamp, a current sensing switch is required in the power supply to instantaneously disconnect the starter.

3.2.3 Gas Cooling Convector

Special cooling gas paths control the flow of gas across the quartz bulb of the arc lamp. Controlled symmetrical forced convection provided by this system eliminates arc wander caused by uneven lamp envelope cooling.

3.2.4 Aconic Collector

The high efficiency 22-inch aconic collector is positioned around the light source to collect the light and direct it upon the transfer optics aperture. The collector has a highly durable nickel electroformed optical surface and is overcoated with vacuum deposited aluminum. The collector is fabricated of composite material to provide an optimum combination of heat transfer and strength. Copper cooling tubes are thermally bonded to the outside of the collector to transfer heat to the liquid coolant system.

3.2.5 Energy Absorber

The energy absorber is inserted into the small diameter of the collector to absorb arc imaged energy reflected from the anode which would cause additional heating of the cathode seal. The energy absorber is machined to an analytically determined shape, coated with high temperature resistant black paint and cooled by the liquid coolant system.

3.2.6 Lamp Adjustment Mechanism

An X-Y-Z lamp adjustment mechanism is attached to the cathode end of the lamp and, in conjunction with the anode positioning spider, allows arc adjustment. The adjustment mechanism is designed to be easily operated for quick adjustment of the lamp in the XMH-300 while in operation. Access to the mechanism is through a specially interlocked cover on the source module.

3.3 Safety Interlocks and Instrumentation

The following safety interlocks, instrumentation and controls are provided as a part of the XMH-300 to provide the proper operating conditions while protecting the xenon lamp.

3.3.1 Flow Switch

The water circuit within the source module (see Spectrolab Drawing No. 019958) is equipped with a flow switch to alarm upon low flow rate. Alarm contacts can be connected to an audio or visual circuit or utilizing a Spectrolab module controller.

3.3.2 Light Output Sensor (Optional)

The XMH-300 source module is equipped with a special ultra-linear high intensity photovoltaic cell positioned to measure the direct light output of the light source. This sensor output is wired to connect to the Spectrolab module controller. It can be measured and recorded with a voltmeter during system preventative maintenance to record the condition of the light source.

3.3.3 Lamp Adjust Mechanism Interlock

Removal of the lamp adjust mechanism cover activates an interlc which prevents activation of the 70 KV starter. This system allows quick adjustment of the lamp in an operating source module without exposure to the 70,000 volt starter pulse.

3.4 Utility Requirements

The following summary of utility requirements outlines the interconnections provided with standard Spectrolab water cooled power cables and electrical control cables.

3.4.1 D.C. Lamp Power

Up to 650 amps and 65 volts DC is provided for the lamp anode and cathode by quickly removable Spectrolab liquid coolant carrying power cables, Figure 4B. Power is routed within the module to the anode and cathode with careful attention to assure less than 1 gauss of unsymmetrical magnetic flux at the lamp arc. (See alternate method of power and water cable hook-up, Figure 4A.) See Spectrolab Drawings 019958 and 019142 for plumbing differences between chambers "B" and "D".

3.4.2 Liquid Coolant

Coolant to and from the XMH-300 is GFE. If lamp is Spectrolab supplied the coolant flow requirements are 5.5 GPM at 150 PSIG for the anode, cathode, starter, collector and energy absorber. Coolant temperature at the inlet must be below 100°F for the above flow rates, but should not be colder than 80°F to prevent condensation on the collector surface. See Drawing No. 019958 for coolant flow diagram.

3.4.3 Control and Alarm Cables

Control and alarm cables are required through a single quick disconnect which also includes the 115V power.

3.5 Codes and Standards

3.5.1 All fluid coolant lines shall be designed to meet the National Electric Safety Code.

3.6. Interchangeability

3.6.1 The engineering study revealed that the Spectrolab "B" chamber source module could be fitted into the "D" chamber enclosure (See Fig. 3) requiring only changes in the mounting configuration of the structure to provide interchangeability. The utility connections, also require modification to allow for the "B" chamber to "D" chamber power supply and control console differences. See Figures 4A and 4B.

PREPARED BY: R. Basil	**spectrolab** A Division of textron Inc	PAGE NO. 11 OF
CHECKED BY:		Job No. 3718 REPORT NO.
DATE: 14 JAN. 71	TITLE CHAMBER "D" HOUSING / CHAMBER "B" XMH-300	NASA MSC MODEL NO. HOUSTON

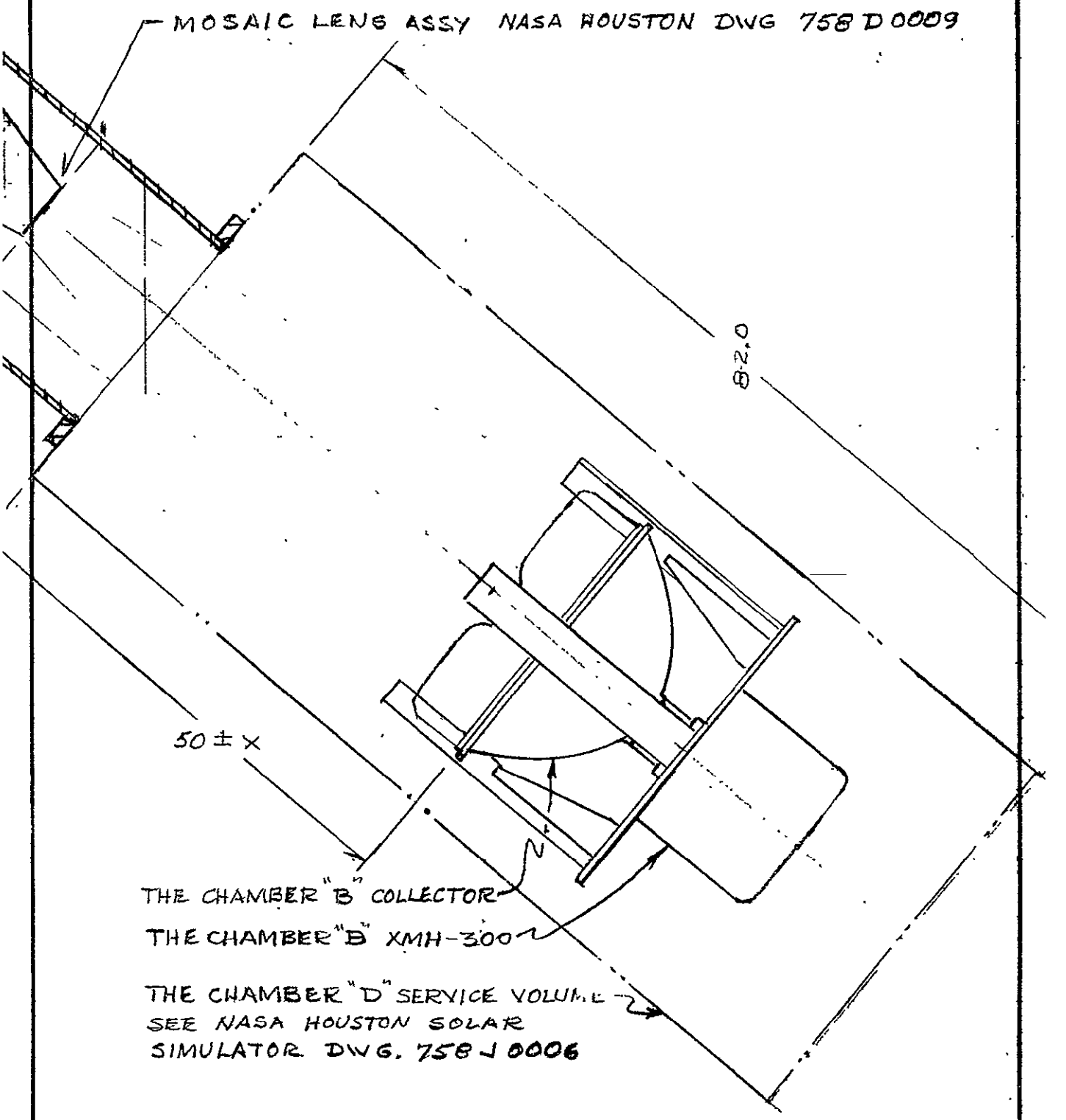

FIG-3

SEE NASA HOUSTON DWG 758-0040 [ASSY- SOURCE/REFLECTOR (24") 20KW RADIATION SOURCE]

3.6.2 Utility interfaces for the "B" chamber XMH-300 source module will require re-design to utilize the present power supply and control console. The degree of re-design to the environmental enclosure could not be evaluated; but should require only an adaptor ring or equivalent.

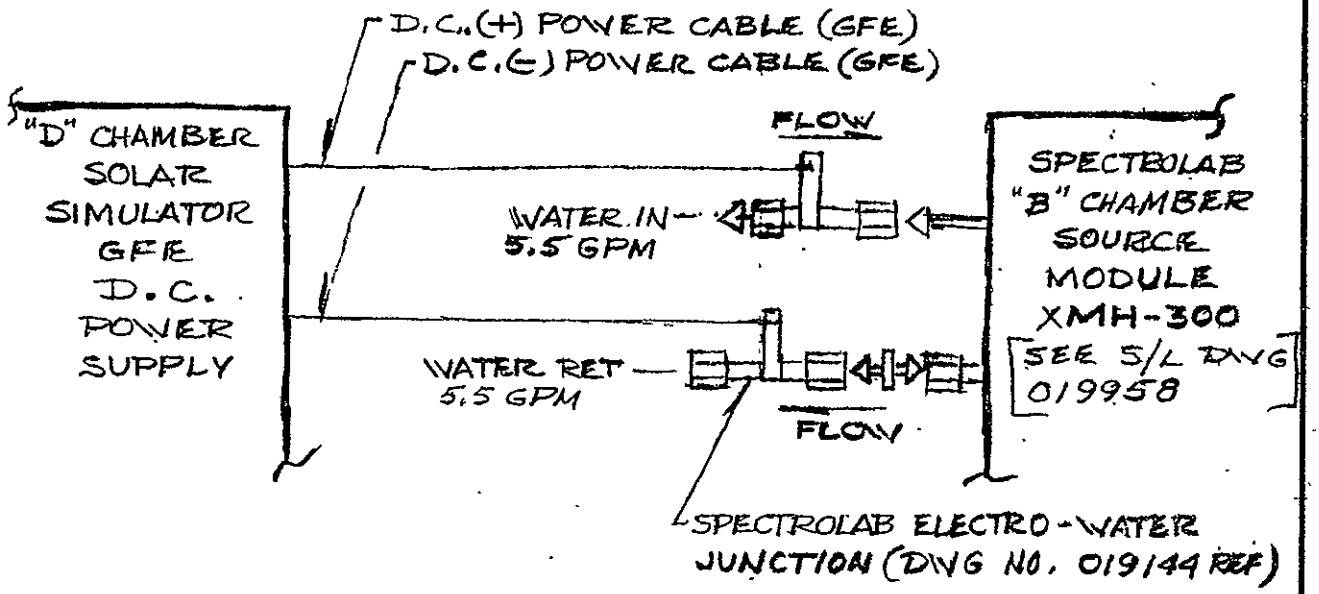

D C POWER FOR "B" CHAMBER XMH-300 WITHOUT WCC

FIG. 4A

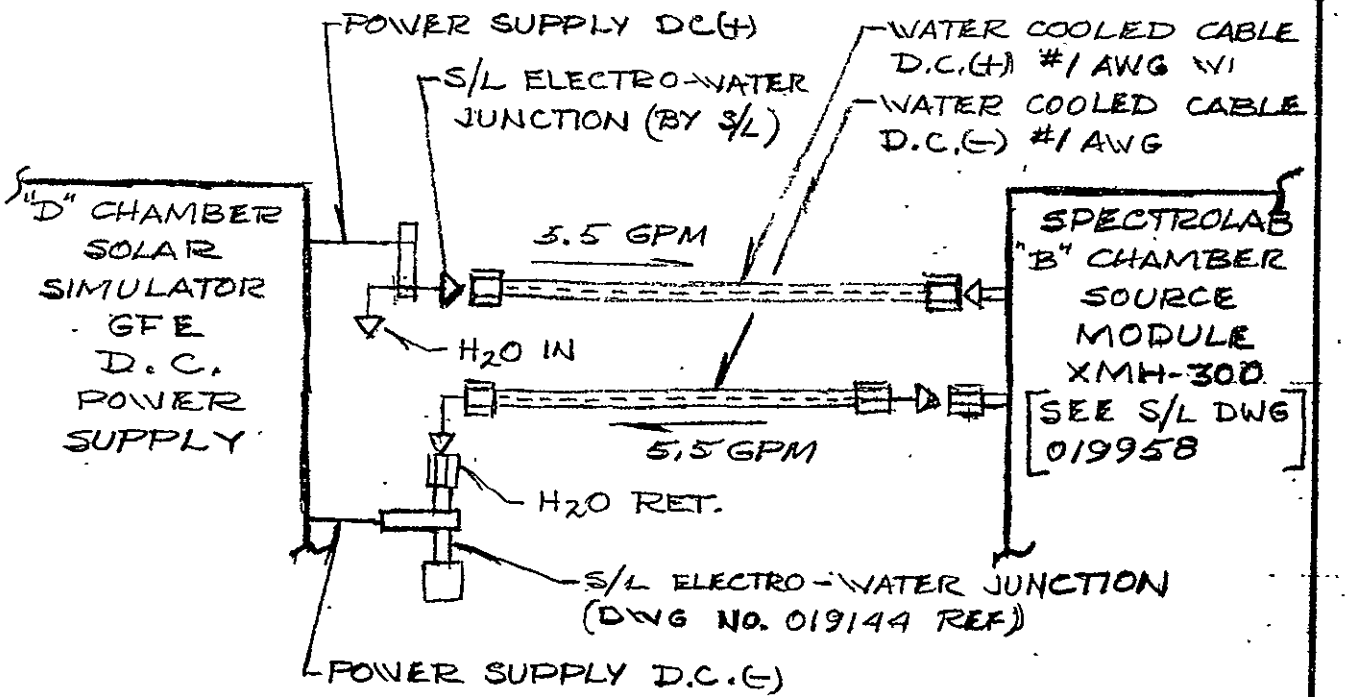

D C POWER FOR "B" CHAMBER WITH WCC

FIG. 4B

APPENDIX A

DEFINITION OF EFFICIENCY FACTORS

1.0 EFFICIENCY FACTORS

The basic efficiency factors which contribute to the overall system efficiency for all approaches considered are described below. The importance of system efficiency cannot be over-emphasized due to its relationship to system cost and test volume irradiance requirements.

Those efficiency factors which make up the total system efficiency are grouped into two basic categories consisting of those factors associated with the conversion of electrical input power to radiation incident on to a circular clear aperture at the transfer optical system, and those associated with the effectiveness of the transfer optical system and collimating optics in transferring the radiation to the test volume.

1.1 SOURCE SYSTEM EFFICIENCY

Those efficiency factors associated with the source system efficiency are defined below:

a. Power Conversion - The conversion factor is defined as the ratio of plasma arc emission transmitted through the quartz envelope to the total electrical input power. The 20 to 30 KW xenon arc source utilizing water-cooled electrodes is the basic source considered in this study. From absolute polar intensity distribution tests conducted at Spectrolab, the power conversion factor has been computed to be in the range of .52 to .58. The lower value of .52 has been selected for use in the system efficiency computations for all approaches.

b. Flux Collection Factor - The fraction of radiation emitted from the lamp that is intercepted by the collector mirror is defined as the flux capture factor. This efficiency factor will also depend to some degree upon the design of the radiation source used, since the solid angle in which the radiation source emits radiation is a function of the electrode configuration. With the latest aero-dynamically designed electrodes, the radiation is emitted over a larger solid angle although none of this additional radiation transmitted from the radiation source is collected by the collecting mirror. This is due to the limited collection angle of the collector which will be on the order of 55° to 130° based upon the angular orientation depicted in Figure A-1.

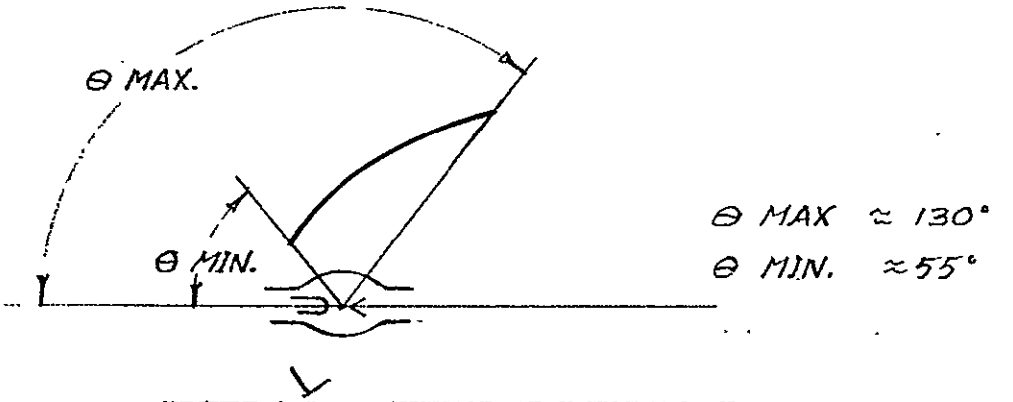

FIGURE A-1. ANGULAR ORIENTATION OF COLLECTION ANGLES

The minimum collection angle is restricted to an angle that will allow for an adequate clearance hole in the rear of the collector for lamp removal. The maximum diameter is established in the collector optimization program.

c. Collector Reflectance - The collector mirror reflectance will depend upon the protective overcoating that is supplied to the vacuum deposited aluminum film. Considerable development work is presently in progress to develop a durable overcoating which can withstand the ultraviolet and ozone environment, provide adequate spectral reflectance characteristics, and withstand normal cleaning maintenance. A value of .86 has been used for the total reflectance value for all mirrors utilized in the various system approaches evaluated.

d. Obstruction Factor - An obstruction factor is utilized to account for usable radiation that is rejected in an optical system due to the presence of physical obstructions in the optical path. An example of such an obstruction are the utility leads to the radiation source that reduce the effective open aperture of the collecting mirror.

Arc Utilization Factor - The ratio of the radiation which strikes a circular aperture circumscribing the field lens elements of the transfer optical system to the total radiation reflected by the collecting mirrors is defined as the arc utilization factor. This efficiency factor will be a function of the collector design, diameter of transfer optics' entrance aperture, collector diameter, and the distance between collector and aperture plane.

OPTICAL TRANSFER EFFICIENCY

Those efficiency factors associated with the transfer optical system in the collimating optics compose the optical transfer efficiency. These factors consist of the following:

a. Packing Factor - The ratio of the radiation incident to the clear aperture of the field lens elements to the total irradiation incident upon the circular aperture circumscribing the field lens elements is defined as the packing factor. The D Chamber system utilizes a 31 element field lens array. If the intensity distribution across the field lens array were uniform, and if the lenses were without chamfers or bevels, the packing factor would be equal to the frontal surface area of the 31 lenses divided by the area of the circumscribing aperture.

b. Lens and Window Transmission Factors - Fused silica or fused quartz is used for window and lens material. The total transmittance of these materials over the spectral range of interest is on the order of .92 depending somewhat upon the thickness of the individual elements. The variations in transmittance is small since the total absorptance for the spectral range of interest is very small per unit thickness. The primary transmission losses are associated with the quartz-air interface reflections.

c. Spectral Filter Factor - For the systems analyzed, it has been assumed that the spectral filter would be deposited upon a separate quartz element rather than deposited upon a lens surface. A filter factor of .70 has been determined from experience to be a realistic value for obtaining a good spectral match.

d. Vignetting and Spillover Factor - Vignetting in a well-designed optical system should be minimu. However, in the design of the quartz lenses, which exhibit a significant change of index of refraction with wavelength, it is necessary to design for a nominal wavelength. Hence, in an optimized designed system some loss of radiation in the near ultraviolet and far-infrared will be experienced at the projection lenses. Also, to insure uniformity of irradiation and spectrum across the test volume, it is necessary to design the system for a slightly larger test volume. The variation of material index or refraction and efficiency gain obtained by minimizing the number of optical components are the primary factors associated with the need to overspill the test volume. The vignetting and spillover factor provide for the accountability for these losses.

APPENDIX B

1.0 ARC UTILIZATION COMPARISON

1.1 Figure 1 illustrates how the "B" chamber source module might be fitted into the enclosure at the solar penetration of "D" chamber. By locating the 22-inch aconic collector at the same distance from the mosaic lenses as the 24-inch ellipsoid any effect upon the decollimation half angle would be minimized.

1.2 To determine optical compatibility of the aconic collector, rays were traced from a pair of points on the optical axis to selected points on the collector and to an image plane at the mosaic lenses. The pair of points on the axis were spaced 12mm apart to represent the typical electrode spacing of a 20 KW lamp. On the collector surface, one point was selected for each 5° zone; the zonal angle was measured between radial lines centered upon the focus of the collector. The intersection with the image plane of rays traced from the two points on the axis through a common point on the collector formed a magnified image of the electrode gap. Using the same procedure, image points were computed for the ellipsoid. Results were plotted on Figure 2.

1.3 The abscissa of Figure 2 is arbitrarily divided into equal spaces in order to permit comparison of the actually superimposed electrode gap images formed by successive zones of the collectors. With the collector zones equally spaced at 5°, the abscissa of Figure 2 represents these angles. Thus, the aconic points which start at 45.020° are offset from the ellipsoid points which start at 43.980° (see Appendix C and D). The ordinate is the elevation, relative to the optical axis of the intersection between a ray and the image plane at the mosaic lenses.

1.4 Two sets of points for the aconic collector were plotted. The difference between the two aconic curves reflects the effect resulting from repositioning the lamp within the collector;

PREPARED BY: AC Brown	spectrolab A Division of Textron Inc	PAGE NO. 19 OF
CHECKED BY:		Job No. REPORT NO. 3718-12-20
DATE:	TITLE OPTICAL SYSTEM INTERFACE	MODEL NO.

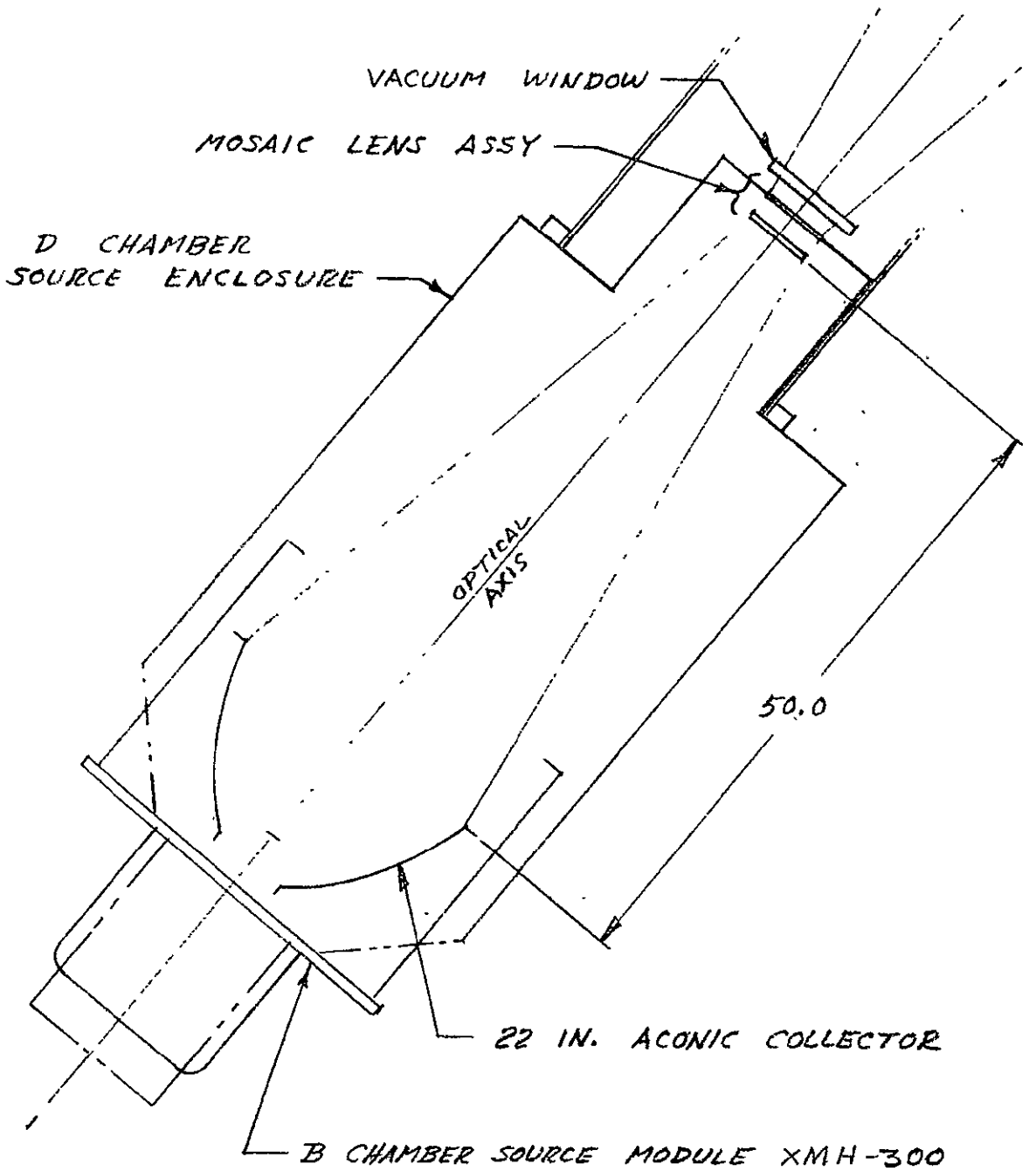

FIGURE 1, APPENDIX B

2.0 mm = 1.0 in.

PREPARED BY: AC Brown	spectrolab A Division of textron Inc	PAGE NO. 20 OF
CHECKED BY:		Job No. REPORT NO. 3718-12-20
DATE:	TITLE ARC UTILIZATION	MODEL NO.

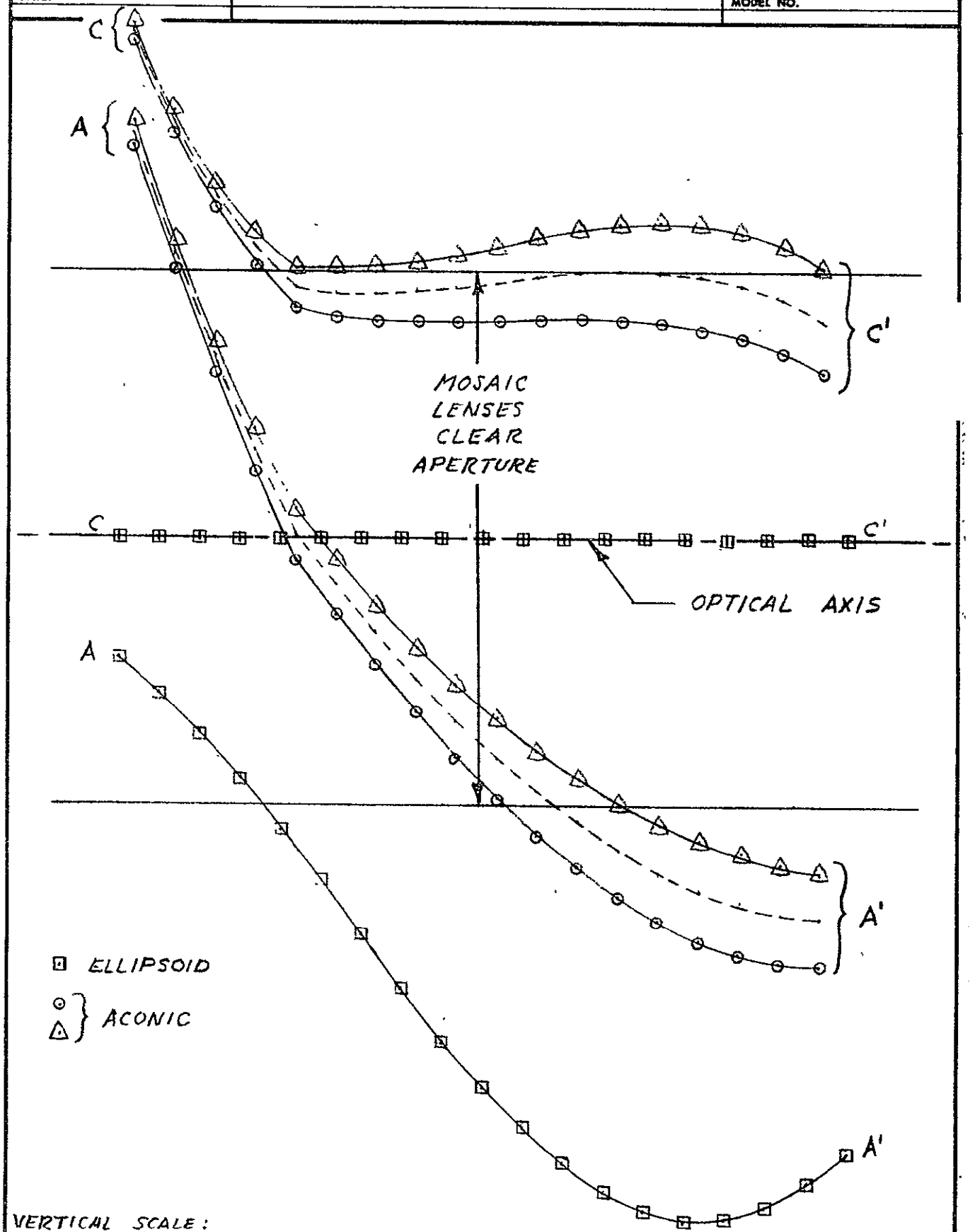

VERTICAL SCALE:
2.0 cm. = 1.0 in.

FIGURE 2, APPENDIX B

S-69-116

the dotted curve was interpolated to illustrate an optimum positioning of the lamp. One set of points for the ellipsoid was plotted based on Section 10.3.5 of the chamber "D" Solar Installation Procedure, which indicates that the lamp is located with the cathode at the focus, and the anode toward the large end of the ellipsoid. The ray trace was based upon this configuration; as a result, the cathode points for the ellipsoid lie along the optical axis.

1.5 Perusal of Figure 2 leads to the conclusion that the energy throughput of the aconic collector is less than that of the ellipsoid. Points which lie outside the region indicated as the mosaic lens clear aperture indicate energy lost to the system. Therefore, the intensity of the arc varies from high at the cathode to low at the anode, "C" points outside the clear aperture represent a much larger loss of energy than do the "A" points.

Again, referring to the curves for the aconic collector, the energy loss for the pair of "triangle" curves is greater than that for the "circle" pair; i.e., the gain from the more intense cathode end of the arc exceeds the loss from the less intense anode end of the arc.

1.6 While the more rigorous investigation required to determine the relative energy ratio of the two different collectors is beyond the scope of this report, it was estimated that the loss of energy entailed through the use of the "B" chamber source module should not exceed 20%.

1.7 Appendix A consists of a set of computer ray trace printouts from which the points of Figure 2 were taken. Data which was plotted is marked on the applicable copies.

3718-12-20; NASA/MSC/HOUSTON, FREE STUDY.

POINTS FOR 24 IN ELLIPSOID (REF. FIGURE 2, APPENDIX B)

TILT ANGLE = 0.00000 DEGREES

COLLECTOR FACE TO CONJUGATE FOCAL PLANE = 50.00000

FIELD LENS DIAM (DF) = 5.00000

SEMI-INTERFOCAL LENGTH = 31.00000

SEMI-MAJOR AXIS = 34.00000

ECCENTRICITY = 0.91176

Z COORDINATES OF RAYS = 62.00000

ORIGIN AT FOCUS ARC LENGTH = 0.47244

PT	ANGLE DEG	RADIUS	AY	AZ	R1Y (C)	R2Y (A)	ARC IMAGE LENGTH	RATIO ARCIM/DF	THEORET MAGNIF
1	43.980	16.6764	11.5803	11.9999	0.0000	-1.0627	1.0628	0.2125	3.0776
2	48.980	14.2813	10.7750	9.3730	0.0000	-1.4062	1.4062	0.2812	3.7614
3	53.980	12.3651	10.0011	7.2714	0.0000	-1.7982	1.7982	0.3596	4.4993
4	58.980	10.8184	9.2713	5.5750	0.0000	-2.2325	2.2326	0.4465	5.2855
5	63.980	9.5583	8.5895	4.1930	0.0000	-2.7005	2.7006	0.5401	6.1142
6	68.980	8.5224	7.9553	3.0568	0.0000	-3.1912	3.1913	0.6382	6.9789
7	73.980	7.6635	7.3659	2.1148	0.0000	-3.6917	3.6917	0.7383	7.8731
8	78.980	6.9457	6.8177	1.3276	0.0000	-4.1876	4.1877	0.8375	8.7901
9	83.980	6.3416	6.3066	0.6650	0.0000	-4.6640	4.6641	0.9328	9.7227
10	88.980	5.8298	5.8289	0.1037	0.0000	-5.1059	5.1059	1.0211	10.6640
11	93.980	5.3938	5.3808	-0.3744	0.0000	-5.4986	5.4986	1.0997	11.6068
12	98.980	5.0207	4.9591	-0.7837	0.0000	-5.8290	5.8290	1.1658	12.5438
13	103.980	4.6999	4.5607	-1.1354	0.0000	-6.0856	6.0856	1.2171	13.4680
14	108.980	4.4235	4.1829	-1.4387	0.0000	-6.2591	6.2592	1.2518	14.3724
15	113.980	4.1846	3.8234	-1.7007	0.0000	-6.3429	6.3430	1.2686	15.2500
16	118.980	3.9779	3.4798	-1.9273	0.0000	-6.3327	6.3327	1.2665	16.0941
17	123.980	3.7992	3.1504	-2.1234	0.0000	-6.2268	6.2269	1.2453	16.8984
18	128.980	3.6448	2.8333	-2.2927	0.0000	-6.0262	6.0262	1.2052	17.6567
19	133.980	3.5118	2.5270	-2.4386	0.0000	-5.7336	5.7337	1.1467	18.3632
20	138.980	3.3978	2.2300	-2.5636	0.0000	-5.3539	5.3540	1.0708	19.0126
21	143.980	3.3009	1.9411	-2.6698	0.0000	-4.8936	4.8937	0.9787	19.5999
22	148.980	3.2195	1.6591	-2.7591	0.0000	-4.3603	4.3603	0.8720	20.1207
23	153.980	3.1523	1.3828	-2.8328	0.0000	-3.7627	3.7627	0.7525	20.5710
24	158.980	3.0983	1.1113	-2.8921	0.0000	-3.1103	3.1104	0.6220	20.9473
25	163.980	3.0566	0.8435	-2.9379	0.0000	-2.4131	2.4131	0.4826	21.2469
26	168.980	3.0266	0.5785	-2.9708	0.0000	-1.6814	1.6814	0.3362	21.4673
27	173.980	3.0079	0.3154	-2.9913	0.0000	-0.9258	0.9259	0.1851	21.6071
28	178.980	3.0002	0.0533	-2.9997	0.0000	-0.1574	0.1574	0.0314	21.6650

3 3718, NASA MSC HOUSTON CH-'3ER D

AS MARKED FOR FIGURE 2, APPENDIX B

TILT ANGLE = -5.73249 DEGREES

COLLECTOR FACE TO CONJUGATE FOCAL PLANE = 179.09780

FIELD LENS DIAM (DF) = 5.00000

SEMI-INTERFOCAL LENGTH = 91.99154

SEMI-MAJOR AXIS = 95.24736

ECCENTRICITY = 0.96581

Z COORDINATES OF RAYS = 183.06298

IGIN AT FOCUS ARC LENGTH = -0.23622

T	ANGLE DEG	RADIUS	AY	AZ	R1Y	R2Y	ARC IMAGE LENGTH	RATIO ARCIM/DF	THEORET MAGNIF
1	65.020	9.3896	8.5114	3.9651	-18.3767	-14.2580	-4.1187	-0.8237	19.2878
2	60.020	10.6075	9.1883	5.3004	-18.3766	-14.9138	-3.4627	-0.6925	16.9583
3	55.020	12.1188	9.9297	6.9474	-18.3766	-15.5301	-2.8464	-0.5692	14.7181
4	50.020	14.0210	10.7440	9.0086	-18.3766	-16.0982	-2.2804	-0.4560	12.5863
5	45.020	16.4546	11.6394	11.6309	-18.3766	-16.6033	-1.7732	-0.3546	10.5749

AUXILIARY PLANE AT Z = 53.96516

PT	YI1R	YI2R	YI1R-YI2R	YDIF/DF
1	1.0048	2.1547	-1.1498	-0.2299
2	1.6420	2.5900	-0.9479	-0.1895
3	2.3727	3.1326	-0.7599	-0.1519
4	3.2224	3.8114	-0.5890	-0.1178
5	4.2271	4.6650	-0.4379	-0.0875

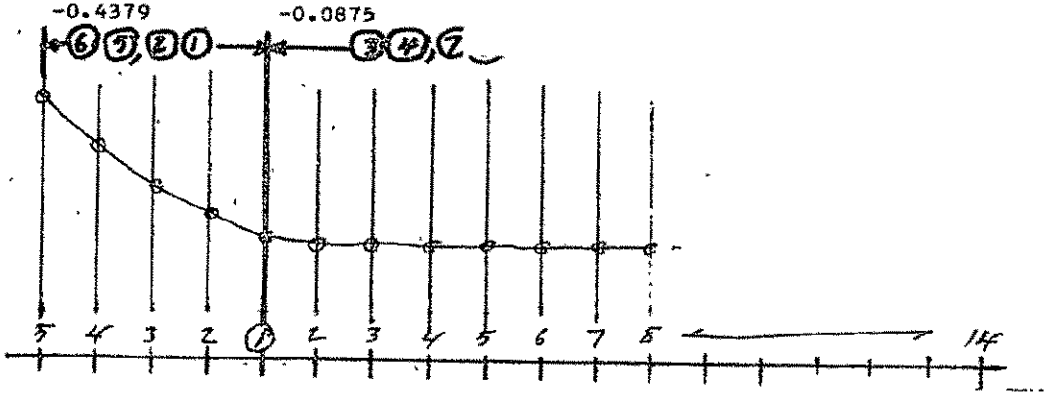

CLCTR 71-0031, 26 JAN 71, 22 IN. COLLECTOR

JOB 3718, NASA MSC HOUSTON CHAMBER D

TILT ANGLE = -5.73249 DEGREES

COLLECTOR FACE TO CONJUGATE FOCAL PLANE = 179.09780

FIELD LENS DIAM (DF) = 5.00000

SEMI-INTERFOCAL LENGTH = 91.99154

SEMI-MAJOR AXIS = 95.24736

ECCENTRICITY = 0.96581

Z COORDINATES OF RAYS = 183.06298

ORIGIN AT FOCUS ARC LENGTH = 0.23622

PT	ANGLE DEG	RADIUS	AY	AZ	R1Y	R2Y	ARC IMAGE LENGTH	RATIO ARCIM/DF	THEORET MAGNIF
1	65.020	9.3896	8.5114	3.9651	-18.3767	-22.6122	4.2354	0.8470	19.2876
2	60.020	10.6075	9.1883	5.3004	-18.3766	-21.9380	3.5614	0.7122	16.9583
3	55.020	12.1188	9.9297	6.9474	-18.3766	-21.3020	2.9254	0.5850	14.7189
4	50.020	14.0210	10.7440	9.0086	-18.3766	-20.7167	2.3401	0.4680	12.5863
5	45.020	16.4546	11.6394	11.6309	-18.3766	-20.1922	1.8156	0.3631	10.5769

AUXILIARY PLANE AT Z = 53.96516

PT	Y1R	Y2R	Y1R-Y2R	YDIF/DF
1	1.0048	-0.1775	1.1824	0.2364
2	1.6420	0.6671	0.9749	0.1949
3	2.3727	1.5917	0.7810	0.1562
4	3.2224	2.6180	0.6044	0.1208
5	4.2271	3.7787	0.4483	0.0896

5 "A" POINTS

JOB 3718, NASA MSC HOUSTON CHAMBER D

TILT ANGLE = -2.40138 DEGREES

COLLECTOR FACE TO CONJUGATE FOCAL PLANE = 80.20614

FIELD LENS DIAM (DF) = 5.00000

SEMI-INTERFOCAL LENGTH = 42.12265

SEMI-MAJOR AXIS = 45.24736

ECCENTRICITY = 0.93094

Z COORDINATES OF RAYS = 84.17131

ORIGIN AT FOCUS ARC LENGTH = 0.23(

PT	ANGLE DEG	RADIUS	AY	AZ	R1Y	R2Y	ARC IMAGE LENGTH	RATIO ARCIM/DF	THEORET MAGNIF
1	65.020	9.3897	8.5114	3.9651	.5297	-5.4265	1.8967	0.3793	8.6376
2	70.020	8.3933	7.8882	2.8678	.5297	-5.7521	2.2224	0.4444	9.7816
3	75.020	7.5678	7.3106	1.9560	.5297	-6.0825	2.5528	0.5105	10.9578
4	80.020	6.8780	6.7739	1.1918	.5297	-6.4089	2.8791	0.5758	12.1571
5	85.020	6.2973	6.2735	0.5465	.5297	-6.7220	3.1923	0.6384	13.3703
6	90.020	5.8052	5.8052	-0.0021	.5297	-7.0127	3.4829	0.6965	14.5884
7	95.020	5.3859	5.3652	-0.4713	-3.5297	-7.2715	3.7417	0.7483	15.8020
8	100.020	5.0269	4.9502	-0.8747	-3.5297	-7.4902	3.9604	0.7920	17.0019
9	105.020	4.7184	4.5572	-1.2228	-3.5297	-7.6612	4.1314	0.8262	18.1789
10	110.020	4.4525	4.1835	-1.5244	-3.5297	-7.7780	4.2482	0.8496	19.3241
11	115.020	4.2230	3.8267	-1.7861	-3.5297	-7.8354	4.3056	0.8611	20.4287
12	120.020	4.0247	3.4848	-2.0136	-3.5297	-7.8300	4.3003	0.8600	21.4844
13	125.020	3.8535	3.1558	-2.2114	-3.5297	-7.7598	4.2300	0.8460	22.4831
14	130.020	3.7061	2.8382	-2.3833	-3.5297	-7.6243	4.0946	0.8189	23.4173

AUXILIARY PLANE AT Z = 53.96516

PT	YI1R	YI2R	YI1R-YI2R	YDIF/DF
1	1.0050	-0.1774	1.1824	0.2364
2	0.7122	-0.6844	1.3967	0.2793
3	0.4530	-1.1618	1.6148	0.3229
4	0.2209	-1.6101	1.8311	0.3662
5	0.0112	-2.0279	2.0392	0.4078
6	-0.1798	-2.4129	2.2330	0.4466
7	-0.3554	-2.7618	2.4064	0.4812
8	-0.5178	-3.0717	2.5538	0.5107
9	-0.6691	-3.3392	2.6700	0.5340
10	-0.8109	-3.5617	2.7508	0.5501
11	-0.9446	-3.7372	2.7926	0.5585
12	-1.0712	-3.8644	2.7931	0.5586
13	-1.1919	-3.9428	2.7509	0.5501
14	-1.3074	-3.9731	2.6656	0.5331

⊙ "A" PTS

CLCTR 71-0031, 26 JAN 71, 22 IN. COLLEC

JOB 3718, NASA MSC HOUSTON CHAMBER D

TILT ANGLE = -5.73249 DEGREES

COLLECTOR FACE TO CONJUGATE FOCAL PLANE = 179.09780

FIELD LENS DIAM (DF) = 5.00000

SEMI-INTERFOCAL LENGTH = 91.99154

SEMI-MAJOR AXIS = 95.24736

ECCENTRICITY = 0.96581

Z COORDINATES OF RAYS = 183.06

ORIGIN AT FOCUS ARC LENGTH = -0.31496

PT	ANGLE DEG	RADIUS	AY	AZ	R1Y	R2Y	ARC IMAGE LENGTH	RATIO ARCIM/DF	THEORET MAGNIF
1	65.020	9.3896	8.5114	3.9651	-18.3767	-12.9104	-5.4663	-1.0932	19.2876
2	60.020	10.6075	9.1883	5.3004	-18.3766	-13.7809	-4.5956	-0.9191	16.9583
3	55.020	12.1188	9.9297	6.9474	-18.3766	-14.5985	-3.7781	-0.7556	14.7189
4	50.020	14.0210	10.7440	9.0086	-18.3766	-15.3489	-3.0276	-0.6055	12.5863
5	45.020	16.4546	11.6394	11.6309	-18.3766	-16.0215	-2.3550	-0.4710	10.5769

AUXILIARY PLANE AT Z = 53.96516

PT	Y11R	Y12R	Y11R-Y12R	Y01F/DF
1	1.0048	2.5309	-1.5260	-0.3052
2	1.6420	2.9002	-1.2581	-0.2516
3	2.3727	3.3813	-1.0086	-0.2017
4	3.2224	4.0044	-0.7820	-0.1564
5	4.2271	4.8087	-0.5815	-0.1163

Δ "C" PTS.

CLCTR 71-0031, 26 JAN 71, 22 IN. COLLECTOR

JOB 3718, NASA MSC HOUSTON CHAMBER D

TILT ANGLE = -5.73249 DEGREES

COLLECTOR FACE TO CONJUGATE FOCAL PLANE = 179.09780

FIELD LENS DIAM (DF) = 5.00000

SEMI-INTERFOCAL LENGTH = 91.99154

(6) SEMI-MAJOR AXIS = 95.24736

ECCENTRICITY = 0.96581

Z COORDINATES OF RAYS = 183.06298

ORIGIN AT FOCUS ARC LENGTH = 0.15748

PT	ANGLE DEG	RADIUS	AY	AZ	R1Y	R2Y	ARC IMAGE LENGTH	RATIO ARCIM/DF	THEORET MAGNIF
1	65.020	9.3896	8.5114	3.9651	-18.3767	-21.1869	2.8101	0.5620	19.2876
2	60.020	10.6075	9.1883	5.3004	-18.3766	-20.7395	2.3628	0.4725	16.9583
3	55.020	12.1188	9.9297	6.9474	-18.3766	-20.3178	1.9412	0.3882	14.7189
4	50.020	14.0210	10.7440	9.0086	-18.3766	-19.9298	1.5532	0.3106	2.5863
5	45.020	16.4546	11.6394	11.6309	-18.3766	-19.5822	1.2055	0.2411	0.5769

AUXILIARY PLANE AT Z = 53.96516

PT	Y11R	Y12R	Y11R-Y12R	YDIF/DF
1	1.0048	0.2203	0.7845	0.1569
2	1.6420	0.9952	0.6468	0.1293
3	2.3727	1.8544	0.5182	0.1036
4	3.2224	2.8212	0.4011	0.0802
5	4.2271	3.9294	0.2977	0.0595

Δ "A" pts

* * * * *

JOB 3718, NASA MSC HOUSTON CHAMBER B

TILT ANGLE = -2.40138 DEGREES

COLLECTOR FACE TO CONJUGATE FOCAL PLANE = 80.20614

FIELD LENS DIAM (DF) = 5.00000

SEMI-INTERFOCAL LENGTH = 42.12265

SEMI-MAJOR AXIS = 43.24736

ECCENTRICITY = 0.93094

Z COORDINATES OF RAYS = 84.17131

ORIGIN AT FOCUS ARC LENGTH = -0.31496

PT	ANGLE DEG	RADIUS	AY	AZ	R1Y	R2Y	ARC IMAGE LENGTH	RATIO ARCIM/DF	THEORET MAGNIF
1	65.020	9.3897	8.5114	3.9651	3.5297	-1.0817	-2.4480	-0.4896	8.6376
2	70.020	8.3933	7.8882	2.8678	3.5297	-0.6569	-2.8728	-0.5745	9.7816
3	75.020	7.5678	7.3106	1.9560	3.5297	-0.2199	-3.3097	-0.6619	10.9576
4	80.020	6.8780	6.7739	1.1918	3.5297	0.2196	-3.7493	-0.7498	12.1571
5	85.020	6.2973	6.2735	0.5465	3.5297	0.6517	-4.1815	-0.8363	13.3703
6	90.020	5.8052	5.8052	-0.0021	3.5297	1.0656	-4.5954	-0.9190	14.5884
7	95.020	5.3859	5.3652	-0.4713	3.5297	1.4503	-4.9801	-0.9960	15.8020
8	100.020	5.0269	4.9502	-0.8747	3.5297	1.7948	-5.3246	-1.0649	17.0019
9	105.020	4.7184	4.5572	-1.2228	3.5297	2.0877	-5.6175	-1.1235	18.1789
10	110.020	4.4525	4.1835	-1.5244	3.5297	2.3184	-5.8482	-1.1696	19.3241
11	115.020	4.2230	3.8267	-1.7861	3.5297	2.4765	-6.0063	-1.2012	20.4287
12	120.020	4.0247	3.4848	-2.0136	3.5297	2.5530	-6.0828	-1.2165	21.4844
13	125.020	3.8535	3.1558	-2.2114	3.5297	2.5398	-6.0696	-1.2139	22.4831
14	130.020	3.7061	2.8382	-2.3833	3.5297	2.4309	-5.9607	-1.1921	23.4173

AUXILIARY PLANE AT Z = 53.96516

PT	Y11R	Y12R	Y11R-Y12R	YDIF/DF
1	1.0050	2.5310	-1.5260	-0.3052
2	0.7122	2.5178	-1.8055	-0.3611
3	0.4530	2.5468	-2.0937	-0.4187
4	0.2209	2.6055	-2.3845	-0.4769
5	0.0112	2.6823	-2.6710	-0.5342
6	-0.1798	2.7664	-2.9463	-0.5892
7	-0.3554	2.8474	-3.2029	0.6405
8	-0.5178	2.9155	-3.4334	0.6866
9	-0.6691	2.9612	-3.6304	0.7260
10	-0.8109	2.9758	-3.7868	0.7573
11	-0.9446	2.9510	-3.8956	0.7791
12	-1.0712	2.8796	-3.9509	0.7901
13	-1.1919	2.7552	-3.9472	0.7894
14	-1.3074	2.5730	-3.8805	0.7761

Δ "C" PTS

UB 3718, NASA MSC HOUSTON CHAMBER D

TILT ANGLE = -2.40138 DEGREES

COLLECTOR FACE TO CONJUGATE FOCAL PLANE = 80.20614

FIELD LENS DIAM (DF) = 5.00000

SEMI-INTERFOCAL LENGTH = 42.12265

SEMI-MAJOR AXIS = 45.24736

ECCENTRICITY = 0.93094

Z COORDINATES OF RAYS = 84.17131

ORIGIN AT FOCUS ARC LENGTH = 0.15748

PT	ANGLE DEG	RADIUS	AY	AZ	R1Y	R2Y	ARC IMAGE LENGTH	RATIC ARCIM/DF	THEORET MAGNIF
1	65.020	9.3897	8.511	3.9651	-3.5297	-4.7882	1.2584	0.2516	8.637
2	70.020	8.3933	7.888	2.8678	-3.5297	-5.0047	1.4749	0.2949	9.781
3	75.020	7.5678	7.310	1.9560	-3.5297	-5.2247	1.6949	0.3389	10.957
4	80.020	6.8780	6.773	1.1918	-3.5297	-5.4426	1.9129	0.3825	12.157
5	85.020	6.2973	6.273	0.5465	-3.5297	-5.6525	2.1227	0.4245	13.370
6	90.020	5.8052	5.805	0.0021	-3.5297	-5.8482	2.3184	0.4636	14.588
7	95.020	5.3859	5.365	0.4713	-3.5297	-6.0236	2.4938	0.4987	15.802
8	100.020	5.0269	4.950	0.8747	-3.5297	-6.1732	2.6434	0.5286	17.001
9	105.020	4.7184	4.557	1.2228	-3.5297	-6.2917	2.7619	0.5523	18.178
10	110.020	4.4525	4.183	1.5244	-3.5297	-6.3747	2.8449	0.5689	19.324
11	115.020	4.2230	3.826	1.7861	-3.5297	-6.4185	2.8887	0.5777	20.428
12	120.020	4.0247	3.484	2.0136	-3.5297	-6.4204	2.8906	0.5781	21.484
13	125.020	3.8535	3.155	2.2114	-3.5297	-6.3786	2.8488	0.5697	22.483
14	130.020	3.7061	2.838	2.3833	-3.5297	-6.2926	2.7629	0.5525	23.417

AUXILIARY PLANE AT Z = 53.96516

PT	Y1R	Y1	Y1R-Y2R	YDIF/DF
1	1.0050	0.2204	0.7845	0.1569
2	0.7122	-0.2146	0.9269	0.1853
3	0.4530	-0.6191	1.0722	0.2144
4	0.2209	-0.9955	1.2165	0.2433
5	0.0112	-1.3446	1.3559	0.2711
6	-0.1798	-1.6663	1.4864	0.2972
7	-0.3554	-1.9593	1.6038	0.3207
8	-0.5178	-2.2224	1.7045	0.3409
9	-0.6691	-2.4541	1.7849	0.3569
10	-0.8109	-2.6531	1.8421	0.3684
11	-0.9446	-2.8182	1.8736	0.3747
12	-1.0712	-2.9488	1.8775	0.3755
13	-1.1919	-3.0446	1.8526	0.3705
14	-1.3074	-3.1061	1.7987	0.3597

A "A" 89..